J|A|C|S
ARTICLES
Published on Web 01/21/2004

S═N versus S^+—N^-: An Experimental and Theoretical Charge Density Study

D. Leusser,[†] J. Henn,[‡] N. Kocher,[†] B. Engels,*[,‡,§] and D. Stalke*[,†,||]

Contribution from the Institutes of Inorganic and Organic Chemistry, Julius-Maximilians-University of Würzburg, Am Hubland, 97074 Würzburg, Germany

Received October 8, 2003; E-mail: bernd@chemie.uni-wuerzburg.de; dstalke@chemie.uni-wuerzburg.de

Abstract: To elucidate the bonding situation in the widely discussed hypervalent sulfur nitrogen species, the charge density distributions $\rho(\mathbf{r})$ and related properties of four representative compounds, methyl(diimido)-sulfinic acid $H(NtBu)_2SMe$ (**1**), methylene-bis(triimido)sulfonic acid $H_2C\{S(NtBu)_2(NHtBu)\}_2$ (**2**), sulfurdiimide $S(NtBu)_2$ (**3**), and sulfurtriimide $S(NtBu)_3$ (**4**), were determined experimentally by high-resolution low-temperature X-ray diffraction experiments ($T = 100$ K). This set of molecules represents an ideal frame of reference for the comparison of SN bonding modes, because they contain short formal S═N double bonds as well as long S—N single bonds, some of them influenced by inter- or intramolecular hydrogen bonds. For comparison, the gas-phase ab initio calculations of the four model compounds, $H(NMe)_2SMe$, $H_2C\{S(NMe)_2(NHMe)\}_2$, $S(NMe)_2$, and $S(NMe)_3$, were performed. The topological features were found to be not particularly sensitive with respect to different substituents R (R = H, Me, *t*Bu). In this paper, it is documented that theory and experiment differ in the eigenvalues of the Hessian matrix because of systematically differing positions of the bond critical points but agree very well concerning the spatial Laplacian distribution and the distinct polarization of all investigated sulfur—nitrogen bonds. Both recommend the S^+—N^- formulation of sulfur nitrogen bonds in **1** and **2** since all nitrogen atoms are found to be sp^3 hybridized. The planar SN_x ($x = 2$, 3) units in the diimide **3** and the triimide **4** reveal characteristics of *m*-center-*n*-electron systems. For none of the investigated S—N bonds, a classical double bond formulation can be supported. This is further substantiated by the NBO/NRT approach. Valence expansion to more than eight electrons at the sulfur atom can definitely be excluded to explain the bonding.

1. Introduction

Since the landmark synthesis of the first sulfurdiimide $S(NR)_2$ in 1956 by Goehring and Weis[1] and the first sulfurtriimide $S(NR)_3$ 14 years later by Glemser and Wegener,[2] the description of the bonding situation has attracted attention. As imide analogues of SO_2 and SO_3, they immediately were celebrated examples of valence expansion at the sulfur atom, not obeying the eight-electron rule. Since the structural characterization of $S(NtBu)_2$[3] and $S(NtBu)_3$[4] revealed very short distances for the sulfur—nitrogen bonds of approximately 1.5 Å, this led to the formulation of S═N double bonds in those compounds.[5] This description avoids formal charges (Pauling's verdict) but implies valence expansion and d-orbital participation at the central sulfur atom. However, this formulation is in contrast to theoretical investigations from the mid 1980s, which verified that d-orbitals cannot participate in the sulfur—nitrogen bonding due to large energy differences between the sulfur p- and d-orbitals.[6] Furthermore, these MO-calculations on second-row atoms in "hypervalent" molecules showed that the d-orbitals are mainly needed as polarization functions rather than as bonding orbitals.[7,8] Theoretical studies of SO_2 and SO_3 show that the S—O bonds have highly ionic character and bond orders close to one. It was demonstrated by Cioslowski et al. that the octet rule even in these molecules is not violated and it is unnecessary to invoke the term of "hypervalency".[9]

A different bonding mode first was suggested by Rundle.[10] He pointed out that the planarity of the SN_x units allows the formation of a delocalized π-electron system leading to *m*-center-*n*-electron bonding.[11] Several experimental observations in recent years[12] do not suit the idea of a classical S═N double

[†] Institute of Inorganic Chemistry, Julius-Maximilians-University of Würzburg.
[‡] Institute of Organic Chemistry, Julius-Maximilians-University of Würzburg.
[§] Author for correspondence regarding theory.
[||] Author for correspondence regarding experiment.

(1) Goehring, M.; Weis, G. *Angew. Chem.* **1956**, *68*, 678.
(2) Glemser, O.; Wegener, J. *Angew. Chem.* **1970**, *82*, 324; *Angew. Chem., Int. Ed. Engl.* **1970**, *9*, 309.
(3) Herberhold, M.; Gerstmann, S.; Milius, W.; Wrackmeyer, B.; Borrmann, H. *Phosphorus, Sulfur Silicon Relat. Elem.* **1996**, *112*, 261.
(4) Pohl, S.; Krebs, B.; Seyer, U.; Henkel, G. *Chem. Ber.* **1979**, *112*, 1751.
(5) Mayer, I. *THEOCHEM* **1987**, *149*, 81.
(6) (a) Kutzelnigg, W. *Angew. Chem.* **1984**, *96*, 262; *Angew. Chem., Int. Ed. Engl.* **1984**, *23*, 272. (b) Reed, A. E.; Weinhold, F. *J. Am. Chem. Soc.* **1986**, *108*, 3586. (c) Bors, D. A.; Streitwieser, A. *J. Am. Chem. Soc.* **1986**, *108*, 1397. (d) Reed, A. E.; Schleyer, P. v. R. *J. Am. Chem. Soc.* **1990**, *112*, 1434. (e) Salzner, U.; Schleyer, P. v. R. *J. Am. Chem. Soc.* **1993**, *115*, 10231. (f) Dobado, J. A.; Martinez-García, H.; Molina, J. M.; Sundberg, M. R. *J. Am. Chem. Soc.* **1998**, *120*, 8461. (g) Stefan, T.; Janoschek, R. *J. Mol. Model.* **2000**, *6*, 282.
(7) Cruickshank, D. W. J.; Eisenstein, M. *J. Mol. Struct.* **1985**, *130*, 143.
(8) Cruickshank, D. W. J. *J. Mol. Struct.* **1985**, *130*, 177.
(9) (a) Cioslowski, J.; Sarján, P. R. *THEOCHEM* **1992**, *255*, 9. (b) Cioslowski, J.; Mixon, S. T. *Inorg. Chem.* **1993**, *32*, 3209.
(10) (a) Rundle, R. E. *J. Am. Chem. Soc.* **1947**, *69*, 1327. (b) Rundle, R. E. *J. Chem. Phys.* **1949**, *17*, 671. (c) Rundle, R. E. *J. Phys. Chem.* **1957**, *61*, 45.
(11) Steudel, R. *Chemie der Nichtmetalle*; deGruyter: Berlin, 1998.

Scheme 1. Textbook Canonical Forms of **1**−**4**

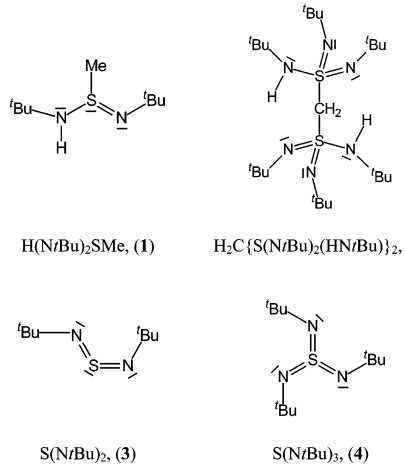

H(N*t*Bu)$_2$SMe, (**1**) $H_2C\{S(N\mathit{t}Bu)_2(HN\mathit{t}Bu)\}_2$, (**2**)

S(N*t*Bu)$_2$, (**3**) S(N*t*Bu)$_3$, (**4**)

bond, e.g., the reactivity of many polyimido sulfur species in polar media. They easily perform transimidation reactions[12d] and generate diimides[13] or the S−N bond inserts into an M−C bond.[14] Since such reactions require facile S−N bond cleavage in polar media, the reactivities indicate a quite polar bonding rather than $p_\pi-d_\pi$ double bonding. Furthermore, the reassignment of the SN stretching vibrations in the Raman spectroscopic experiment to much lower wavenumbers (640 and 920 cm^{-1} [13] instead of initially assumed 1200 cm^{-1} [15−17]) indicates a weaker bond and probably another bonding type rather than S═N.

To elucidate the characters of the different SN bonds in the present study, we use the atoms in molecules (AIM) method[18] and the NBO/NRT approach[19] to analyze and compare the electron density distributions of methyl(diimido)sulfinic acid H(N*t*Bu)$_2$SMe (**1**), methylene-bis(triimido)sulfonic acid $H_2C\{S(N\mathit{t}Bu)_2(HN\mathit{t}Bu)\}_2$ (**2**), sulfurdiimide S(N*t*Bu)$_2$ (**3**), and sulfurtriimide S(N*t*Bu)$_3$ (**4**) depicted in Scheme 1.

Experimental electron densities were determined from single-crystal high-resolution X-ray diffraction data, while the theoretical counterparts were obtained from DFT approaches employing large atomic basis sets. The selection of molecules is well suited for this study, since it covers a wide range of different SN bonds and contains sulfur atoms in the formal oxidation states +IV and +VI. Additionally, the influence of weak interactions such as inter- and intramolecular hydrogen bridges on the bonding between nitrogen and sulfur atoms can be studied. While some aspects were already discussed for $H_2C\{S(N\mathit{t}Bu)_2(HN\mathit{t}Bu)\}_2$ (**2**),[20] a thorough comparative study was still missing. Furthermore, while previous studies elaborate more indirect indicators (vibrational spectra, geometrical features, chemical reactivity), the present study is based on the interpretation of experimentally and theoretically determined electron density distributions.

The routine low-resolution X-ray structures of H(N*t*Bu)$_2$SMe (**1**)[13] and S(N*t*Bu)$_3$ (**4**)[4] are known, but a detailed investigation of their bonding properties on the basis of the electron density was missing. Contrary to the chemistry of sulfurdiimides,[21] the chemistry of sulfurtriimides is rather unexplored[22] due to the up to recently synthetically limited access.[12c] In early studies, the SN vibrations of sulfurtriimides in the region around 1200 cm^{-1} were used to witness S═N double bonds, but unambiguous signal assignment, achieved by DFT methods, proves that they appear at much lower wavenumbers, indicating a much weaker bond and probably another bonding type.[13] Hence, chemical and spectroscopical evidence stimulates the present study of the charge density distribution in these target molecules.

Both S^{IV} species H(N*t*Bu)$_2$SMe (**1**) and S(N*t*Bu)$_2$ (**3**) contain formal S═N double bonds. While in **1** a localized formal double bond and a single bond coexist, in **3** both SN formal double bonds are chemically equivalent. Interestingly they differ geometrically. Although former studies concentrated on chemical aspects and standard molecular geometries and properties, profound experimental charge density studies and their theoretical counterparts were required. The density distribution of methylene-bis(triimido)sulfonic acid $H_2C\{S(N\mathit{t}Bu)_2(HN\mathit{t}Bu)\}_2$ (**2**) obtained from high-resolution X-ray diffraction experiments which is already communicated[20] nevertheless is included in the present work for comparison purposes. This paper extends the initial work by the theoretically determined electron densities.

2. Experimental Details

Diffraction data for all compounds were collected on a Bruker Apex-CCD diffractometer equipped with a low-temperature N_2 gas stream device at 100 K.[23] The data were collected in an omega-scan mode ($\Delta\omega = -0.2°, -0.3°$) at fixed φ-angles with a detector to a sample distance of 5 cm at exposure times of 4 to 15 s for the low-angle reflections and 40 to 200 s for the high-angle reflections, respectively. This gives high-resolution data ($\sin\theta/\lambda \geq 1.11$ $Å^{-1}$) at redundancies of 3 to almost 10 depending on the Laue symmetry. The data collection was monitored with SMART,[24] and the integration was performed with SAINT[25] using the 3d profiling method described by Kabsch[26] and corrected for absorption with MULABS implemented in PLATON[27] using the Blessing algorithm.[28,29]

(12) (a) Fleischer, R.; Freitag, S.; Pauer, F.; Stalke, D. *Angew. Chem.* **1996**, *108*, 208. *Angew. Chem., Int. Ed. Engl.* **1996**, *35*, 204. (b) Fleischer, R.; Rothenberger, A.; Stalke, D. *Angew. Chem.* **1997**, *109*, 1140; *Angew. Chem., Int. Ed. Engl.* **1997**, *36*, 1105. (c) Fleischer, R.; Freitag, S.; Stalke, D. *J. Chem. Soc., Dalton Trans.* **1998**, 193. (d) Fleischer, R.; Stalke, D. *Organometallics* **1998**, *17*, 832. (e) Fleischer, R.; Stalke, D. *J. Chem. Soc., Chem. Commun.* **1998**, 343. (f) Fleischer, R.; Stalke, D. *J. Organomet. Chem.* **1998**, *550*, 173. (g) Ilge, D.; Wright, D. S.; Stalke, D. *Chem.—Eur. J.* **1998**, *4*, 2275. (h) Walfort, B.; Lameyer, L.; Weiss, W.; Herbst-Irmer, R.; Bertermann, R.; Rocha, J.; Stalke, D. *Chem.—Eur. J.* **2001**, *7*, 1417. (i) Walfort, B.; Pandey, S. K.; Stalke, D. *J. Chem. Soc., Chem. Commun.* **2001**, 1640.
(13) Fleischer, R.; Walfort, B.:, Gburek, A.; Scholz, P.; Kiefer, W.; Stalke, D. *Chem.—Eur. J.* **1998**, *4*, 2259.
(14) Walfort, B.; Leedham, A. P.; Russell, C. A.; Stalke, D. *Inorg. Chem.* **2001**, *40*, 5668.
(15) Glemser, O.; Pohl, S.; Tesky, F. M.; Mews, R. *Angew. Chem.* **1977**, *89*, 829; *Angew. Chem., Int. Ed. Engl.* **1977**, *16*, 789.
(16) Meij, R.; Oskam, A.; Stufkens, D. J. *J. Mol. Struct.* **1979**, *51*, 37.
(17) (a) Herbrechtsmeier, A.; Schnepel, F. M.; Glemser, O. *J. Mol. Struct.* **1978**, *50*, 43. (b) Markowskii, L. N.; Tovstenko, V. I.; Pashinnik, V. E.; Mel'nichuk, E. A.; Makarenko, A. G.; Shermolovich, Yu. G. *Zh. Org. Khim.* **1991**, *27*, 769 (tansl.).
(18) Bader, R. F. W. *Atoms in Molecules: A Quantum Theory*; Oxford University Press: Oxford, 1990.
(19) Glendening, E. D.; Badenhoop, J. K.; Reed, A. E.; Carpenter, J. E.; Weinhold, F. *NBO 4.M*; Theoretical Chemistry Institute, University of Wisconsin, Madison, WI, 1999.
(20) Leusser, D.; Walfort, B.; Stalke, D. *Angew. Chem.* **2002**, *114*, 2183; *Angew. Chem., Int. Ed.* **2002**, *41*, 2079.
(21) Reviews: (a) Fleischer, R.; Stalke, D. *Coord. Chem. Rev.* **1998**, *176*, 431. (b) Stalke, D. *Proc. Indian Acad. Sci. (Chem. Sci.)* **2000**, *112*, 155.
(22) Review: Mews, R.; Watson, P. G.; Lork, E. *Coord. Chem. Rev.* **1997**, *158*, 233.
(23) (a) Stalke, D. *Chem. Soc. Rev.* **1998**, *27*, 171. (b) Kottke, T.; Stalke, D. J. *Appl. Crystallogr.* **1993**, *26*, 615. (c) Kottke, T.; Lagow, R. J.; Stalke, D. *J. Appl. Crystallogr.* **1996**, *29*, 465.
(24) *SMART-NT: Program for Diffractometer Controlling*; Bruker Nonius Inc.: Madison, WI, 2000.
(25) *SAINT-NT: Program for Integration of Diffraction Data from Area Detectors*; Bruker Nonius Inc.: Madison, WI, 2000.
(26) Kabsch, W. *J. Appl. Crystallogr.* **1988**, *21*, 916.
(27) Spek, A. L. *Acta Crystallogr.* **1990**, *A46*, C-34.
(28) Blessing, B. *Acta Crystallogr.* **1995**, *A51*, 33.

3. Refinement

All structures were solved with SHELXS,[30] and conventional refinements using all data were performed with SHELXL-97.[31,32] The multipole refinements on F^2 data were performed using the atom-centered multipole model by Hansen and Coppens.[33] The starting atomic parameters were received by a spherical atom refinement.[34] The parameters of the non-hydrogen atoms were determined by high-order refinement ($\sin\theta/\lambda \geq 0.8$, **3**, or 1.0 Å^{-1}, **1**, **2**, **4**), and those of the hydrogen atoms, by exclusive use of the low-angle data ($\sin\theta/\lambda \leq 0.5$ Å^{-1}) and a riding model for the isotropical thermal motion parameters. After refinement, the hydrogen atoms were shifted along their bonding vectors to neutron diffraction distances.[35] For S(N*t*Bu)$_2$, **3**, application of an anharmonic thermal motion model by a Gram−Charlier expansion[36] to the fourth order for the central sulfur atom led to a significant improvement. A comparable situation for a sulfur-containing compound was already observed by Lecomte et al.,[37] and the application of an anharmonic motion model was discussed in detail there. Multipole refinements were carried out on F^2 with the full-matrix-least-squares refinement program XDLSM implemented in the XD package.[38] The core and the spherical valence densities were composed of Hartree−Fock wave functions expanded over Slater-type basis functions. For the deformation density terms, single-ζ orbitals with energy-optimized Slater exponents were used.[39] The expansions over the spherical harmonics were truncated at the hexadecapolar level for the sulfur, nitrogen, and sulfur-bonded carbon atoms and for the other carbon atoms at the octapolar level. The hydrogen atoms were represented by a bond directed dipole and quadrupole term. Chemically equivalent and symmetry related atoms were constrained to share the same expansion/contraction parameters and multipole populations. Several local noncrystallographic symmetry restrictions were applied for the angular functions. The density parameters were implemented in the refinement routines in a stepwise manner, but in the final cycles, all parameters were refined together using positive reflections without any intensity over sigma restrictions until convergence was reached.[40]

4. Theoretical Details

Gas-phase structures of the model compounds were optimized for different substituents R=H, Me, and *t*Bu, respectively, employing a great variety of theoretical methods. Stationary points were checked by frequency calculations. With respect to the basis set, the computed densities are converged at the 6-311G** level. The variations obtained as a function of the theoretical approach were also small if correlation effects were included either via the MP2 formalism or via DFT. Substituent effects on SN bond topological as well as on NBO/NRT properties are also small. The typical changes of the densities at the bond critical points (BCPs) are below 0.2 e/Å^3, and a detailed analysis of these small changes indicated that, e.g., the hybridization state of the sulfur and nitrogen centers are qualitatively not affected. Consequently, in the present paper we concentrate on the results obtained at the DFT B3PW91/6-311G** level of theory with R = Me. All calculations were performed with the Gaussian98 package.[41] The topological analyses were performed with the AIM2000 package,[42] while the NBO/NRT analyses were performed with the NBO 4.0

(29) Crystal data for **1**, **3**, and **4** (data of **2** are given in ref 20): The data were collected in omega-scan mode from shock-cooled crystals using graphite-monochromated Mo Kα radiation (λ = 0.710 73 Å) at 100(2) K. Data collections were performed in two independent batches, a low-angle ($2\Theta_{detector} = -31°$) and a high-angle batch ($2\Theta_{detector} = -80°$), respectively. The resulting data sets were assigned an individual scaling factor and were treated independently during all steps of data processing. The small overlap region was not employed to scale both batches. This strategy allows a maximum resolution limit of up to $\sin\Theta/\lambda$ = 1.14 Å^{-1} from only two batches of data. **1**: $C_9H_{22}N_2S_1$, M = 190.35, monoclinic, space group $P2_1/c$, a = 8.8832(3) Å, b = 14.7504(5) Å, c = 9.3656(3) Å, β = 110.8510(10)°, V = 1146.81(7) Å^3, Z = 4, ρ_{calcd} = 1.102 mg/m^3, μ = 0.240 mm^{-1}, $F(000)$ = 424, 54 868 reflections measured (low-angle batch, $\sin\theta/\lambda$ < 0.625 Å^{-1}), R(int) = 0.0567, 42 875 reflections measured (high-angle batch, 0.625 Å^{-1} < $\sin\theta/\lambda$ < 1.111 Å^{-1}), R(int) = 0.0300, 14 000 unique reflections. **3**: $C_8H_{18}N_2S_1$, M = 175.31, triclinic, space group $P1$, a = 5.9699(3) Å, b = 9.2877(4) Å, c = 9.9338(4) Å, α = 72.5050(10)°, β = 88.3380(10)°, γ = 84.6610(10)°, V = 523.04(4) Å^3, Z = 2, ρ_{calcd} = 1.113 mg/m^3, μ = 0.258 mm^{-1}, $F(000)$ = 194, 12 299 reflections measured (low-angle batch, $\sin\theta/\lambda$ < 0.625 Å^{-1}), R(int) = 0.0461, 25 532 reflections measured (high-angle batch, 0.625 Å^{-1} < $\sin\theta/\lambda$ < 1.111 Å^{-1}), R(int) = 0.0540, 11 808 unique reflections. **4**: $C_{12}H_{27}N_3S_1$, M = 245.43, triclinic, space group $P1$, a = 9.3228(3) Å, b = 9.3455(3) Å, c = 10.6675(3) Å, α = 70.5150(10)°, β = 77.5710(10)°, γ = 60.5540(10)°, V = 761.52(4) Å^3, Z = 2, ρ_{calcd} = 1.070 mg/m^3, μ = 0.196 mm^{-1}, $F(000)$ = 272, 17 996 reflections measured (low-angle batch, $\sin\theta/\lambda$ < 0.625 Å^{-1}), R(int) = 0.0287, 44 864 reflections measured (high-angle batch, 0.625 Å^{-1} < $\sin\theta/\lambda$ < 1.111 Å^{-1}), R(int) = 0.0307, 18 250 unique reflections.

(30) Sheldrick, G. M. *Acta Crystallogr*. **1990**, *A46*, 467.

(31) *SHELXTL-97*; Bruker Nonius Inc.: Madison, WI, 1997.

(32) Refinement of **1**, **3**, and **4** (conventional/IAM refinement; data of **2** are given in ref 20): The structures were solved by direct methods and refined by full-matrix least-squares methods against F^2. R values defined as $R1 = \Sigma||F_o| - |F_c||/\Sigma|F_o|$, $wR2 = [\Sigma w(F_o^2 - F_c^2)^2/\Sigma w(F_o^2)^2]^{0.5}$, $w = [\sigma^2(F_o^2) + (g_1P)^2 + g_2P]^{-1}$, $P = 1/3[\max(F_o^2, 0) + 2F_c^2]$. **1**: $C_9H_{22}N_2S_1$, *wR2*(all data) = 0.0691, *R1*($I > 2\sigma(I)$) = 0.0277, g_1 = 0.043, g_2 = 0.0 for 176 parameters. **3**: $C_8H_{18}N_2S_1$, *wR2*(all data) = 0.0820, *R1*($I > 2\sigma(I)$) = 0.0324, g_1 = 0.049, g_2 = 0.0 for 155 parameters. **4**: $C_{12}H_{27}N_3S_1$, *wR2*(all data) = 0.0750, *R1*($I > 2\sigma(I)$) = 0.0280, g_1 = 0.050, g_2 = 0.0 for 227 parameters. All hydrogen atoms were located by difference Fourier synthesis and refined without any distance restraints. The isotropic displacement parameters of the hydrogen atoms were refined using a riding model ($U_{iso} = 1.2U_{eq}$ (N) for the nitrogen bonded hydrogen atom H1 in **1** and $U_{iso} = 1.5U_{eq}$ (C) for all other hydrogen atoms). Crystallographic data (excluding structure factors) for the structures reported in this paper have been deposited with the Cambridge Crystallographic Data Centre as supplementary publication no. 196159 (**1**), CCDC-171901 (**2**), CCDC-191359 (**3**), and CCDC-191360 (**4**). Copies of the data can be obtained free of charge on application to CCDC, 12 Union Road, Cambridge CB2 1EZ, UK [Fax: (internat.) + 44(1223)-336-033. E-mail: deposit@ccdc.cam.ac.uk].

(33) Hansen, N. K.; Coppens, P. *Acta Crystallogr*. **1978**, *A34*, 909.

(34) Refinement of a starting model for subsequent multipole refinements: Positional and anisotropic displacement parameters of the non-hydrogen atoms were refined by using exclusively reflections with $\sin\theta/\lambda \geq 1.0$ Å^{-1} (**1**, **2**, **4**) or $\sin\theta/\lambda \geq 0.8$ Å^{-1} (**3**) due to application of an anharmonic motion model for sulfur by a Gram−Charlier expansion to the fourth order with 25 extra parameters in **3**. During high-order refinement, a $1/\sigma^2$ (F^2) weight was used. The isotropic displacement parameters of the hydrogen atoms were refined using a riding model ($U_{iso} = 1.2\ U_{eq}$ (N) for the nitrogen bonded hydrogen atom H1 in **1** and $U_{iso} = 1.5\ U_{eq}$ (C) for all other hydrogen atoms) using reflections with $\sin\theta/\lambda \leq 0.5$ Å^{-1}. After refinement, the hydrogen atoms were shifted along their bonding vector to neutron diffraction distances of 1.085 Å for the H−C(sp^3) and 1.032 Å for the nitrogen bonded H atoms, respectively.

(35) Allen, F. A. *Acta Crystallogr*. **1986**, *B42*, 515.

(36) Johnson, C. K.; Levy, H. A. *International Tables for X-ray Crystallography*; Kynoch Press: Birmingham, 1974; Vol. 4.

(37) Pillet, S.; Souhassou, M.; Pontillon, Y.; Caneschi, A.; Gatteschi, D.; Lecomte, C. *New J. Chem*. **2001**, *25*, 131.

(38) Koritsanszky, T.; Howard, S.; Mallinson, P. R.; Su, Z.; Richter, T.; Hansen, N. K. *XD − A Computer Program Package for Multipole Refinement and Analysis of Electron Densities from Diffraction Data*; Freie Universität Berlin, 1996.

(39) Clementi, E.; Roetti, C. *At. Data Nucl. Data Tables* **1974**, *14*, 177.

(40) Multipole refinements: In the pseudoatom model of the sulfur atoms, recommended n_l values (4, 4, 6, 8 for l = 1, 2, 3, 4) were used for the deformation density model.[33] All compounds were refined with an identical refinement strategy. Chemically equivalent atoms shared the same multipole parameters (methyl hydrogen atoms, peripheral methyl carbon atoms, symmetry related tertiary carbon and nitrogen atoms). In addition, symmetry restrictions were implemented to reduce the number of refinement parameters. (**1**) C_3 symmetry for all methyl groups; (**2**) C_3 symmetry for all methyl groups, C_2 symmetry for the two molecular moieties at the bridging CH_2; (**3**) C_3 symmetry for all methyl groups; (**4**) C_3 symmetry for the complete molecule and all methyl groups. Residuals after multipole refinement: (**1**) w*R1*($I > 3\sigma(I)$) = 0.0210, *wR2*(all data) = 0.0271, GoF = 1.2344, N_{refl}/N_{param} = 53.5; (**2**) w*R1*($I > 3\sigma(I)$) = 0.0147, *wR2*(all data) = 0.0280, GoF = 1.3015, N_{refl}/N_{param} = 67.9; (**3**) w*R1*($I > 3\sigma(I)$) = 0.0203, *wR2*(all data) = 0.0314, GoF = 1.1631, N_{refl}/N_{param} = 44.1; (**4**) w*R1*($I > 3\sigma(I)$) = 0.0180, *wR2*(all data) = 0.0293, GoF = 1.5970, N_{refl}/N_{param} = 82.6. All final difference Fourier syntheses after multipole refinement are virtually featureless.

Table 1. Bond Lengths [Å] (Interatomic Line) and Angles [deg] of **1**−**4**[a]

1	S1−N1	1.6829(2)	N1−S1−N2	110.1(1)	**2**	S1,2−N1,4	1.6494(2)	S1−C7−S2	122.2(1)
		1.7061(7)		109.64(3)			1.6950(1)		120.54
	S1−N2	1.5847(2)	N1−S1−C3	101.9(1)		S1,2−N2,5	1.5279(3)	N1,4-S1,2−N2,5	110.2(3)
		1.5962(2)		102.54(11)			1.5478(1)		118.79(1)
	S1−C3	1.7907(2)	N2−S1−C3	100.0(1)		S1,2−N3,6	1.5177(6)	N1,4−S1,2−N3,6	102.4(3)
		1.8083(1)		99.91(5)			1.5345(1)		109.76(1)
	(N1)H1···X1_N2[b]	2.0271(2)	N1−H1···X1_N2[b]	167.8(1)		S1,2−C7	1.8164(5)	N2,5−S1,2−N3,6	126.8(2)
		1.8596(24)		171.9(1)			1.8364		114.35(1)
3	S1−N1:	1.5437(4)	N1−S1−N2:	117.4(1)		(N1)H1···N5	2.1568(3)	N1,4−S1,2−C7	105.9(1)
		1.5591		114.47			1.8922		96.00(1)
	S1−N2:	1.5279(4)				(N4)H4···N2	2.1379(3)	N2,5−S1,2−C7	100.2(4)
		1.5413					1.8921		101.25(1)
4	S1−N1:	1.5116(2)	N1−S1−N2:	120.2(1)				N3,6−S1,2−C7	110.2(3)
		1.5305		120.01					115.13(1)
	S1−N2:	1.5120(2)	N1−S1−N3:	119.9(1)				N1−H1···N5	142.6(1)
		1.5306		120.00					156.31
	S1−N3:	1.5113(2)	N2−S1−N3:	119.9(1)				N4−H4···N2	142.7(1)
		1.5306		120.00					156.31

[a] In each column, the upper entry denotes experimental values, and the lower entry gives theoretical values from B3PW91/6-311G** calculations on methyl-substituted model compounds. The experimental values of **2** are averaged over the two moieties. Theoretical values of **1** result from averaging of chemically equivalent bonds and thus are given with esd's. [b] X1 = 1 − *x*, −*y*, −*z*.

package.[19] The natural resonance theory (NRT) according to Weinhold et al. is based on the natural bond orbitals (NBO) approach which in turn is the most compact representation of the first-order reduced density matrix. Its diagonal elements refer to atomic orbitals (natural atomic orbitals, NAO), and the off-diagonal elements describe the coupling to the other atoms in the molecule. In the case of weak delocalization, the NRT procedure yields one strong dominating Lewis structure, while in the strong delocalization case, many Lewis structures are calculated, each contributing with its computed weight. The atomic charges, bond orders, valencies, etc. are computed by summing up the weighted contributions of all Lewis structures. For more details, see ref 43.

5. Results and Discussion

The molecular structures of the sulfur−nitrogen compounds as derived from the X-ray experiments after multipole refinement are displayed in Figure 1, while Table 1 gives selected geometrical parameters. In the solid state, dimeric H(N*t*Bu)$_2$SMe (**1**) adopts a twisted boat conformation of an $S_2N_4H_2$ eight-membered ring due to intermolecular hydrogen bonding of H1 to the opposite formally double bonded N2A. The relatively short H1···N2A distance and an almost linear N1−H1···N2A angle indicate a strong hydrogen bond in **1**, which suggests that the dimerization of **1** is an important energetic contribution to the solid-state lattice energy.[44] The sulfur atom in **1** is trigonal pyramidally substituted displaying a stereochemically active lone pair and sp^3 hybridization. Threefold substitution of the nitrogen atom of the S−N(H)R amino residue gives rise to an unambiguous S−N1 single bond of 1.6829(2) Å. The formal S=NR double bond S1=N2 of the imino moiety (1.5847(2) Å) is significantly shorter but 0.07 Å longer than the formal double bonds in S(NR)$_3$, (**4**). At first sight, this bond elongation might be attributed to the hydrogen bond with N2 as the acceptor, but this commonly used argument cannot be sustained in a comparison with **2** where extremely short formal S=N bonds are found, although the nitrogen atoms participate in hydrogen bonds. In **1** the N−C bond lengths are almost equal, while the S−N−C angles differ only slightly (S1−N1−C1 = 119.6(1)° vs S1−N2−C2 = 115.0(1)°). It is remarkable that the trisub-

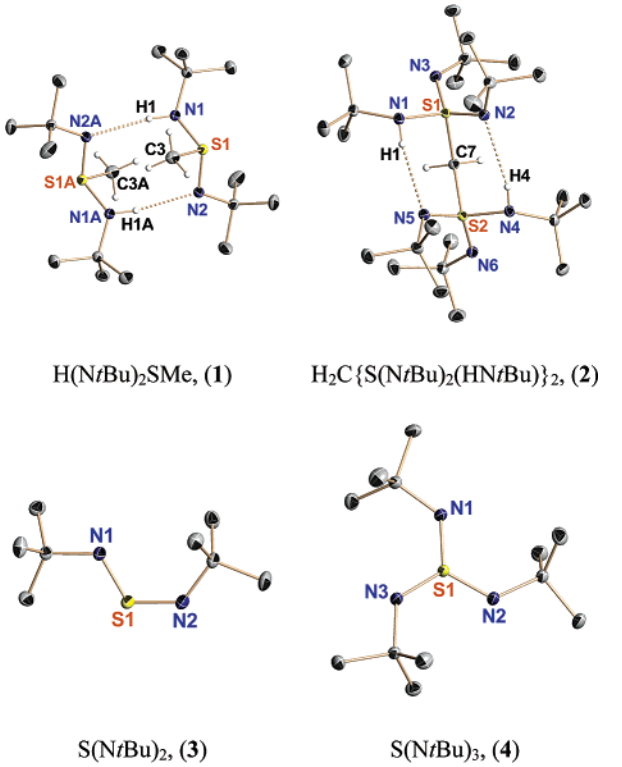

Figure 1. Solid-state structures of **1**−**4**; anisotropic displacement parameters are depicted at the 50% probability level, and C−H bonded hydrogen atoms are omitted for clarity.

(41) Frisch, M. J.; Trucks, G. W.; Schlegel, H. B.; Scuseria, G. E.; Robb, M. A.; Cheeseman, J. R.; Zakrzewski, V. G.; Montgomery, J. A., Jr.; Stratmann, R. E.; Burant, J. C.; Dapprich, S.; Millam, J. M.; Daniels, A. D.; Kudin, K. N.; Strain, M. C.; Farkas, O.; Tomasi, J.; Barone, V.; Cossi, M.; Cammi, R.; Mennucci, B.; Pomelli, C.; Adamo, C.; Clifford, S.; Ochterski, J.; Petersson, G. A.; Ayala, P. Y.; Cui, Q.; Morokuma, K.; Malick, D. K.; Rabuck, A. D.; Raghavachari, K.; Foresman, J. B.; Cioslowski, J.; Ortiz, J. V.; Baboul, A. G.; Stefanov, B. B.; Liu, G.; Liashenko, A.; Piskorz, P.; Komaromi, I.; Gomperts, R.; Martin, R. L.; Fox, D. J.; Keith, T.; Al-Laham, M. A.; Peng, C. Y.; Nanayakkara, A.; Gonzalez, C.; Challacombe, M.; Gill, P. M. W.; Johnson, B.; Chen, W.; Wong, M. W.; Andres, J. L.; Gonzalez, C.; Head-Gordon, M.; Replogle, E. S.; Pople, J. A. *Gaussian 98*, revision A.7; Gaussian, Inc.: Pittsburgh, PA, 1998.
(42) Biegler-König, F.; Schonbohm, J.; Bayles, D. AIM2000 − A Program to Analyze and Visualize Atoms in Molecules. *J. Comput. Chem.* **2001**, *22*, 545.
(43) (a) Glendening, E. D.; Weinhold, F. *J. Comput. Chem.* **1997**, *6*, 593. (b) Glendening, E. D.; Weinhold, F. *J. Comput. Chem.* **1997**, *6*, 610. (c) Glendening, E. D.; Weinhold, F. *J. Comput. Chem.* **1997**, *6*, 628.
(44) Steiner, T. *Angew. Chem.* **2002**, *114*, 50; *Angew. Chem., Int. Ed.* **2002**, *41*, 48.

stituted nitrogen atom N1 shows the wider angle compared to the disubstituted N2. The angle at the potentially sp^3 hybridized N1 should be closer to 109° than those at the potentially sp^2 hybridized N2. However, the relatively narrow angle at N2 might be taken as the first hint that a single in-plane lone pair at N2 is not present in **1**.

The intramolecular S1—N1—H1—N5—S2—N4—H4—N2 ring in **2** forms a boat conformation, bow and stern connected by the methylene bridge. The molecule consists of two $S(NtBu)_2$-(NH*t*Bu) moieties linked by CH_2 and two intramolecular hydrogen bonds. According to the Cahn—Ingold—Prelog rules, the structure of **2** is S/S chiral. Both moieties are almost equal concerning bond lengths and angles, giving rise to a noncrystallographic 2-fold axis through the methylene carbon atom C7 and the center of the S1—C7—S2 unit. The wide S1—C7—S2 angle of 122.2(1)° reflects considerable steric strain between the two bulky methylene substituents. The 4-fold substituted sulfur atoms in **2** obviously are sp^3 hybridized. Like in **1**, different SN bonding modes are observed: two S—N(H) single bonds and four formal S═N double bonds. The N—H···N angles are much smaller than those found for the intermolecular bridge in **1**. The short H···N distances also support the assumption of a strong hydrogen bond. But in contrast to the situation in **1**, the formal S═N(acceptor) bonds in **2** are not that much elongated and match almost exactly the averaged distance in **4** (expt: 1.512(2) Å).

In the solid-state $S(NtBu)_2$ (**3**) adopts a non-*C*s symmetrical *E*/*Z* conformation. All atoms of the SN_2C_2 backbone are almost located in a plane with an average deviation from the mean plane of only 0.005 Å. The formal S═N bonds (1.5279(4) and 1.5437(4) Å) differ 0.016 Å in length, and both are in the range quoted for a double bond.[53] Compared to other SN_2 units, both formal S═N double bonds[45] are in the range of short interactions (e.g., $S(NSiMe_3)_2$[46] 1.516 and 1.523 Å; $S(NSiPh_3)_2$[47] 1.506 and 1.508 Å; $S(NC_6F_5)(NPh)$[48] 1.526 and 1.551 Å; $S(NC_6H_4F\text{-}p)_2$[49] 1.539 and 1.555 Å). The S—N—C angles differ remarkably (expt: 118.3(1)° (*E*) vs 128.1(1)° (*Z*)), where the angle of the *E* substituent is close to the anticipated value of an sp^2 nitrogen atom. The crystal packing of **3** exhibits short S···S distances of 3.5663 (5) Å in the solid state, which are about 0.13 Å shorter than the sum of the van der Waals radii.[50] An analogous arrangement has previously been observed in $Te\{N(SiMe_3)_2\}_2$.[51]

The experimental solid-state structure of $S(NtBu)_3$ (**4**) shows almost exactly C_{3h} symmetry (av N—S—N = 120.0(3)°). The formal S═N bond lengths (expt: av 1.512(2) Å) are slightly shorter compared to those of **3**. This shortening is due to the higher oxidation state of the central sulfur atom (S^{VI} in **3** and S^{IV} in **4**).[12b] However, the formal S═N bond lengths in **4** fall at the short end of the range observed for SN_3 units.[45] The atoms of the $S(NC)_3$ core are located almost in plane. As already discussed by Pohl et al.,[4] a slight trigonal pyramidal arrangement cannot be excluded for the SN_3 unit in the solid-state structure. Relative to the N_3 plane, the central sulfur and the tertiary carbon atoms are shifted toward the same direction, while the in-plane methyl carbon atoms are oriented about the same amount (some hundredth of an angstrøm) in the opposite direction. Pohl and co-workers concluded that this finding is related to extended out-of-plane thermal motion components. The preferred out-of-plane motion perpendicular to atomic bonds is expected from the rigid bond postulate,[52] and a comparison of the principal mean square atomic displacements supports their assumption. The out-of-plane components in **4** are at least 2 times the values of the in-plane motion, which is not the case for **3**. This feature might be attributed to a slight disorder of the SN_3 units in **4** with respect to their mean plane. Due to the relatively low temperature of 100 K, this disorder is assumed to be of static rather than of dynamic nature. The S—N—C angles (expt: av 125.7(5)°) are still in sufficient agreement with the model of sp^2 hybridized nitrogen atoms.

A general comparison of experimental bond lengths (R = *t*Bu) and the corresponding theoretical values obtained for the model systems with R = Me reveals only slight elongations of the theoretical intramolecular bonds (≤0.02 Å). The SN bonds presented in Table 1 can be separated into two classes: short ones with lengths normally quoted for S═N bonds[53] (1.51 Å (S1—N1, **4**) to 1.58 Å (S1—N2, **1**)) and long ones (1.65 to 1.71 Å for S1—N1 in **2** and **1**) with distances in the range of standard S—N single bonds. The textbook canonical structures are presented in Scheme 1. The differences of the intramolecular bonding angles between experiment and theory are also found to be small (≤4°). Larger differences are found for the intermolecular bonding distances of the hydrogen bridges. These deviations may result from the weak interaction compared to intramolecular bonding. Calculated and solid-state bonding angles of **2** also deviate considerably (N2,5—S1,2—N3,6: 127° vs 114°). However, as shown by calculations performed for the optimized geometry and the experimental arrangement, an energetic discrepancy of only 3.8 kcal/mol is found. This indicates that the underlying bending potentials are very flat, for which the steric effects resulting from the *t*Bu groups lead to large changes in the geometrical parameters. Since the change in the geometrical arrangement may also alter the character of the bonding, this issue will be addressed later. The flat bending potentials also explain why N—S—N and S—N—C angles vary in a wide range and do not contain straightforward information about the hybridization states of the centers.

5.1. Topological Analysis and Laplacian Distribution. To obtain more insight in the bonding situation, complete topological analyses were performed for all compounds. (3,−1) bond critical points (BCPs) representing saddle points in the density between two atoms were detected for all bonds. In the topological definition, a chemical bond is represented by the bond path, the gradient path linking two neighboring nuclei along which $\rho(\mathbf{r})$ is a maximum with respect to any neighboring line. The values of the charge densities, $\rho(\mathbf{r}_{BCP})$, the negative Laplacians, $-\nabla^2\rho(\mathbf{r}_{BCP})$, the ellipticities, ϵ_{BCP}, and the eigenvalues of the Hessian matrix, λ_i, at the BCPs are presented in Table 2. According to the atoms in molecules (AIM) theory of Bader, these properties can be used to distinguish between

(45) Cambridge Structural Database, version 5.24, April 2003.
(46) Herberhold, M.; Gerstmann, S.; Wrackmeyer, B.; Borrmann, H. *J. Chem. Soc., Dalton Trans.* **1994**, 633.
(47) Herberhold, M.; Gerstmann, S.; Milius, W.; Wrackmeyer, B.; Borrmann, H. *Phosphorus, Sulfur Silicon Relat. Elem.* **1996**, *112*, 261.
(48) Bagryanskaya, I. Y.; Gatilov, Y. V.; Shakirov, M. M.; Zibarev, A. V. *Mendeleev Commun.* **1994**, 167.
(49) Lork, E.; Mews, R.; Shakirov, M. M.; Watson, P. G.; Zibarev, A. V. *Eur. J. Inorg. Chem.* **2001**, 2123.
(50) Emsley, J. *The Elements*; de Gruyter: New York, 1994.
(51) Björgvinsson, M.; Roesky, H. W.; Pauer, F.; Stalke, D.; Sheldrick, G. M. *Inorg. Chem.* **1990**, *26*, 5140.
(52) Hirshfeld, F. L. *Acta Crystallogr.* **1976**, *A32*, 239.
(53) Rademacher, P. *Strukturen organischer Moleküle*; VCH: Weinheim/New York, 1987.

Table 2. BCP Properties of the S−E (E = N, C) Bonds in Compounds **1**−**4**[a]

		d	d_{BCP}	$\rho(\mathbf{r}_{BCP})$	$-\lambda_1/-\lambda_2/\lambda_3$	$\nabla^2\rho(\mathbf{r}_{BCP})$	ϵ_{BCP}
1	S1−N1	1.683	0.834	1.76(3)	10.26/9.66/11.97	−7.95(8)	0.06
		1.71	0.75	1.43	7.74/7.19/3.69	−11.23	0.08
	S1−N2	1.585	0.769	2.06(3)	12.28/11.32/10.43	−13.17(9)	0.08
		1.60	0.63	1.72	8.65/7.63/10.32	−5.96	0.13
	S1−C3	1.791	0.994	1.54(2)	9.18/8.72/9.20	−8.70(5)	0.05
		1.808	0.973	1.29	7.46/7.04/6.58	−7.92	0.06
2	S1−N1	1.650	0.780	1.89(3)	11.47/10.32/8.38	−13.41(7)	0.11
		1.70	0.74	1.51	8.88/7.92/3.27	−13.53	0.12
	S1−N2	1.530	0.718	2.31(3)	13.61/12.41/9.43	−16.60(9)	0.10
		1.55	0.60	1.86	10.65/8.31/19.35	0.39	0.28
	S1−N3	1.520	0.718	2.37(3)	13.78/13.01/10.36	−16.44(9)	0.06
		1.53	0.60	1.87	10.45/7.96/21.89	3.47	0.31
	S1−C7	1.817	0.984	1.45(2)	8.69/7.95/8.64	−8.01(4)	0.09
		1.836	0.854	1.25	7.26/7.02/6.94	−7.33	0.03
3	S1−N1	1.546	0.681	1.93(3)	9.62/8.99/9.18	−9.44(8)	0.07
		1.56	0.60	1.76	9.78/7.37/22.50	5.34	0.33
	S1−N2	1.531	0.788	2.24(3)	12.58/11.73/14.92	−9.38(7)	0.07
		1.54	0.60	1.80	10.31/7.51/23.96	6.14	0.37
4	S1−N1	1.513	0.738	2.27(3)	14.40/11.83/15.69	−10.56(8)	0.22
		1.53	0.60	1.86	10.91/7.16/21.74	3.67	0.52

[a] In each column, the upper entry denotes experimental values, and the lower entry gives theoretical values from B3PW91/6-311G** calculations on methyl-substituted model compounds. *d* is the bond path length [Å], and d_{BCP} [Å] denotes the distances of the BCP from the sulfur atom. λ_i (i = 1, 2, 3) [e/Å^5] are the eigenvalues of the Hessian matrix, ϵ_{BCP} is the ellipticity, $\rho(\mathbf{r}_{BCP})$ [e/Å^3] is the charge density, and $\nabla^2\rho(\mathbf{r}_{BCP})$ [e/Å^5] is the Laplacian at the BCP.

various types of interactions. Negative values of the Laplacian accompanied by high values of the density at the BCPs are commonly associated with a distinct covalent character of the bond ("shared interactions"), while highly positive values in the Laplacian accompanied by relatively small values of the electron density are attributed to an ionic character of the bond (closed shell interactions). However, for very polar bonds, problems arise if the topology is discussed exclusively at the BCPs.[54,55] The BCPs of such bonds appear in a region where the density distribution is shaped very flat. As a consequence, small changes in the description of $\rho(\mathbf{r})$ already lead to large alterations in the position of the BCPs. One consequence is the considerable difference between theoretically and experimentally determined values.

Since the SN bonds are expected to be polar, similar problems have to be considered, and indeed, for the short SN bonds, the theoretical BCPs are located on roughly one-third of the bond distance from S to N, while the experimental BCPs are found close to the center of the bond path. While the theoretical value is found in the rampant edge of the Laplacian, the experimental BCP appears where the Laplacian is changing smoothly. This difference is less prominent for the long S1−N1 bonds in **1** and **2**. Here the positions and topological values of the theoretical and experimental BCPs correspond better. This indicates a larger polarity of the short SN bonds compared to the single bonds. The shifts of the BCPs hampered the interpretation of the comparison between theoretical and experimental eigenvalues λ_i.[55]

Nevertheless, since the BCP is defined as the point with the lowest density between the bonding partners, both theory and experiment should at least correlate in $\rho(\mathbf{r}_{BCP})$. Indeed, as can be seen from Table 2 and Figure 2, experimental and theoretical

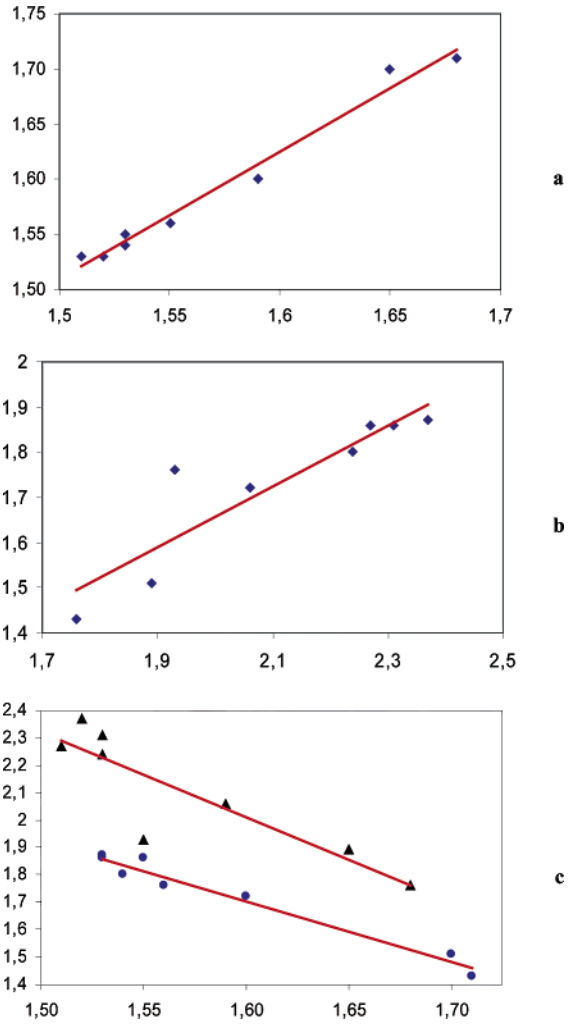

Figure 2. Correlation between theoretical and experimental bond distances and the charge densities at the respective BCPs. (a) Experimental (*x*-axis) vs theoretical (*y*-axis) bond distances of SN bonds in Å. Best fit straight line: $y = 1.154x + 0.223$; coefficient of correlation $R^2 = 0.981$. (b) Experimental (*x*-axis) vs theoretical (*y*-axis) $\rho(\mathbf{r}_{BCP})$. Best fit straight line: $y = 0.677x + 0.303$; coefficient of correlation $R^2 = 0.824$. The outlier is from S1−N1 in **3**. (c) Bond distance (*x*-axis) in Å vs $\rho(\mathbf{r}_{BCP})$ (*y*-axis) in theory (●) and experiment (▲). Again, the outlier originates from the experimental S1−N1 in **3**.

charge densities at the BCPs differ in absolute values but a correlation is obvious. However, Figure 2 also shows one exception for $\rho(\mathbf{r}_{BCP})$ of S1═N1 in **3**. This unexpected value seems to be related to the experimental position of the BCPs, which, compared to the other bonds under investigation, is located extremely close to the sulfur atom. As pointed out in the Experimental Details, the sulfur atom in **3** had to be refined with an anharmonic motion model. Therefore, we assume shortcomings in the experimental model to be responsible for that outlier.

All expected VSCCs (VSCC = valence shell charge concentration) appearing as (3, −3) critical points in the negative Laplacian were found for all experimental as well as theoretical models. These VSCCs are used to identify the lone pairs of the valence shell electron pair repulsion model.[18] For all compounds under study, we found the lone pairs of the nitrogen atoms inclined toward the electropositive sulfur atoms. This effect should be interpreted as lone-pair back-bonding as described by Chesnut.[56] Following this argumentation, the lone pairs can

(54) Bach, A.; Lentz, D.; Luger, P. *J. Phys. Chem.* **2001**, *A 105*, 7405.
(55) Volkov, A.; Abramov, Y.; Coppens, P.; Gatti, C. *Acta Crystallogr.* **2000**, *A56*, 332.

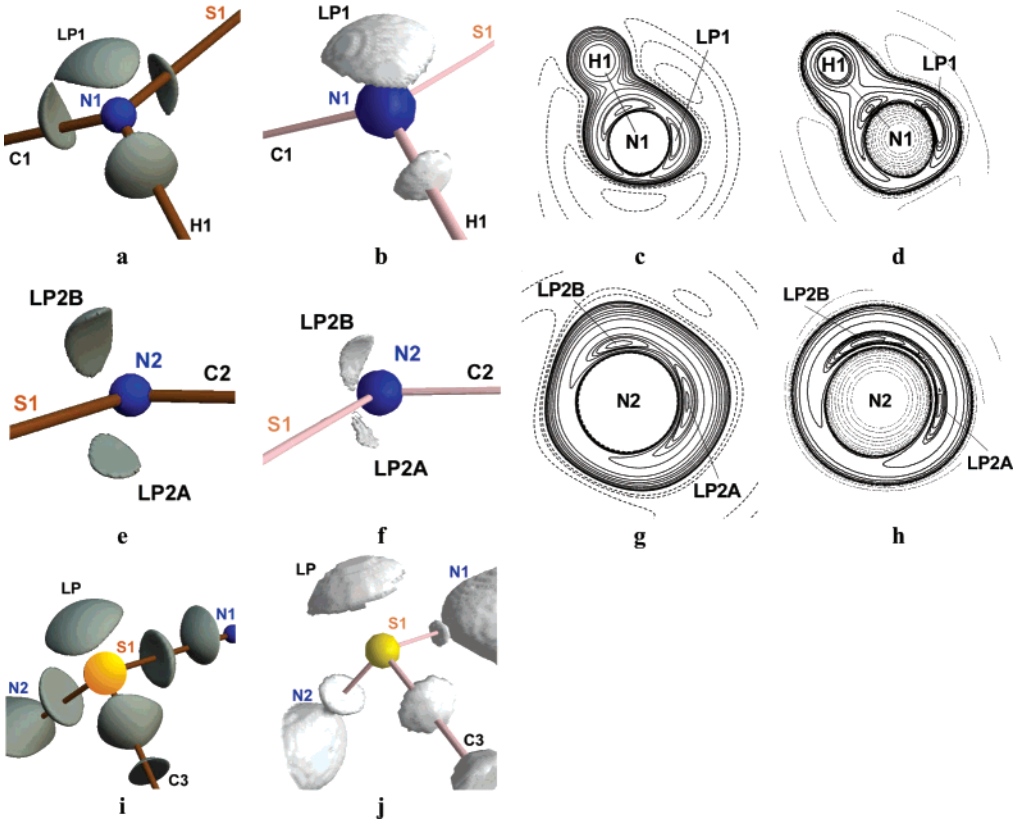

Figure 3. Isosurface ((exptl) a, e, i; (theo) b, f, j) of $-\nabla^2\rho(\mathbf{r})$ and contour plot representations ((exptl) c, g; (theo) d, h) of $\nabla^2\rho(\mathbf{r})$ (solid lines negative, dashed lines positive values) around S1 (i, j), N1 (a−c), and N2 (e−h) in **1**.

contribute to the bonding considerably by an orientation of lone-pair density toward the bonding region.

5.1.1. H(N*t*Bu)$_2$SMe (X-ray) and H(NMe)$_2$SMe (Theory) (1). Compound **1** shows two chemically different nitrogen centers (Figure 1). In the classical interpretation as indicated by the Lewis diagrams in Scheme 1, one would expect a single sulfur amino and a double sulfur imino bond. The S1—N1 σ-type single bond in **1** represents the longest bond path of all studied S—N bonds with the lowest density at the BCPs combined with the smallest ellipticity of the systems under investigation. In contrast to the experimental data, its theoretically determined Laplacian, $\nabla^2\rho(\mathbf{r}_{BCP})$, differs considerably from those of the formal double bonds (see Table 2). Compared to this single bond, the density and ellipticity at the BCPs for S1═N2 is higher. In the experiment, the difference between both SN bonds is reflected by an increased negative Laplacian at the BCPs, while the calculations reveal the opposite trend (Table 2). This results from the differences in the positions of the BCPs, quite common for such polar bonds.[54,55] Despite this, experiment and theory agree in nearly all qualitative features of the spatial distribution of $\nabla^2\rho(\mathbf{r})$. Both exhibit local concentrations of electron density above and below the S1—N2—C2 plane indicating two nonbonding VSCCs (see Figure 3e−h). This is reminiscent of the computed findings in S_4N_4. Bader et al. found in their pioneering theoretical study the same density features (two VSCCs in the bonding and two in the nonbonding region of the nitrogen atoms), which persuaded them to formulate the S—N bond as a S$^+$—N$^-$ bond.[57] However, in an experimental charge density study of S_4N_4, the S—N single bond shortening was attributed to π-contribution.[58] Since one stereochemically active nonbonding VSCC is also found for S1 and N1 (Figure 3a−d, i, j), both experiment and calculations describe all S and N atoms in **1** as predominantly sp^3 hybridized. It is evident from this hybridization state that the S1—N2 interaction cannot be described as an S═N double bond but has to be classified as a highly polar S$^+$—N$^-$ bond.

This interpretation of the bonding situation is supported by the leading resonance structure (weight ≈ 35%) of **1** as obtained from the NBO/NRT analysis (Figure 4). However, the additional two Lewis structures with smaller weights than that in the NBO/NRT give a more subtle picture. They contain S1═N2 double bonds, but the S1—N1 covalent bond found in the leading Lewis structure is cleaved and replaced by an ionic interaction. Please note that this ionic interaction not only covers the polarity one would expect from electronegativity differences for each SN bond but also is induced to some extent from the attempt of N2 to redistribute the negative charge over the whole molecule. In the NBO/NRT interpretation, the sulfur atom forms only two covalent bonds to the nitrogen centers, either one to each neighbor (Figure 4a) or two to the N2 center but as a consequence none to the corresponding N1 (Figure 4b, c). The "third" bond to the nitrogen atom, which appears in the classical interpretation (Scheme 1) is not covalent but arises from ionic interactions. However, as indicated by the less important Lewis structures, this "ionic bonding character" is not limited to the

(56) Chesnut, D. B. *J. Phys. Chem.* **2003**, *A107*, 4307.

(57) Tang, T.-H.; Bader, R. F. W.; MacDougall, P. J. *Inorg. Chem.* **1985**, *24*, 2047.

(58) Scherer, W.; Spiegler, M.; Pedersen, B.; Tafipolsky, M.; Hieringer, W.; Reinhard, B.; Downs, A. J.; McGrady, G. S. *J. Chem. Soc., Chem. Commun.* **2000**, 635.

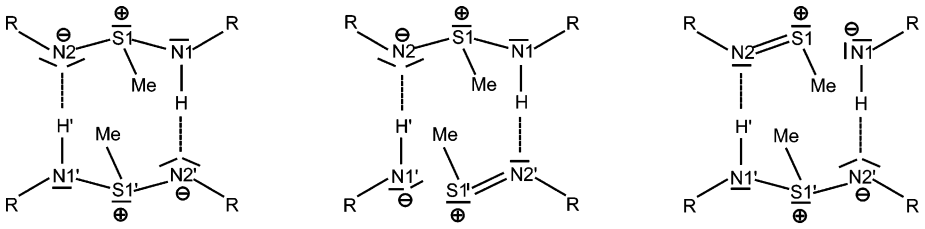

Figure 4. NBO/NRT analysis of **1**. Formal atomic charges: (S1) +1.14 e, (N1) −1.05 e, (N2) −1.18 e. Bond orders: (S1−N1) 0.78 (covalent 0.56, ionic 0.23), (S1−N2) 1.23 (covalent 0.91, ionic 0.32), (S1−C3) 0.95 (covalent 0.93, ionic 0.02). Parts b and c are independent descriptions, as the two $H(NMe)_2SMe$ residues were not constrained to be geometrically equal.

pair S1—N2 but to some extent distributed over the whole SN_2 moiety. As a consequence, also the charge, which in a strictly localized ionic bond would be concentrated at N2, is distributed over both nitrogen atoms. From this model, one expects a polar S1—N1 bond with a covalent bond order considerably lower than one and an increased S1—N2 bond order with higher covalent and at the same time also higher ionic contributions than those in the S1−N1 bond. This is indeed reflected in the bond orders computed by the NBO/NRT approach (Figure 4).

The rationalization provided by the NBO/NRT approach is in complete agreement with the description given by the AIM interpretation of the theoretical density. As already discussed, we find two VSCCs at the N2 atom and one at the sulfur center indicating an S^+N^- pair, but at the same time, the AIM analysis of the theoretical density also describes the S1−N2 bond with a higher ϵ_{BCP} and $\rho(\mathbf{r}_{BCP})$ than those in the S1−N1 bond. This further proves that the charge located at N2 is redistributed to some extent to the SN_2 core. It is important to note that the theoretical $\nabla^2\rho(\mathbf{r}_{BCP})$ gets considerably less negative proceeding from N1−S1 to N2−S1, indicating a more ionic bond. At the same time $\rho(\mathbf{r}_{BCP})$ also increases, which is commonly associated with a predominant covalent bond. In accord to the redistribution description, the lone pairs of the nitrogen atoms are inclined toward the electropositive sulfur atom, leading to lone-pair back-bonding.[56]

The experimental topological parameters at the BCPs provide almost the same model. It is important to note that theoretical and experimental BCPs are located at different positions. Nevertheless, an internal comparison of the SN bonds within one approach (experimental or theoretical) is consistent. In the experiment, the negative value of $\nabla^2\rho(\mathbf{r})$ and the higher density indicate an increase of the covalent character of S1−N2 with respect to S1−N1. The number of VSCCs around the sulfur and the nitrogen atoms, however, lead to an S^+N^- pair. As discussed for the theoretical results, the lone-pair back-bonding is reflected in an inclination of the lone pairs at N2 toward the bonding region.

In both experiment and theory, a redistribution of the charge accumulated at the N2 center is observed; however, it may differ in the extent of the distribution. Theory describes the system in the vacuum for which the localization of charge is even more unfavorable with respect to the energy than in the polar solid-state environment. As a consequence, the redistribution in the present theoretical model is probably more distinct than that in the experiment. The difference should be quite small for **1**, since both theory and experiment agree in the first coordination sphere of the negatively charged nitrogen centers, given by the intermolecular hydrogen bonds. Test calculations about this question are under way. Nevertheless, despite the differences at the BCPs, theory, experiment, AIM, and NBO/NRT analyze a bonding situation which is much closer to $S1^+—N2^-$ than to S1═N2.

5.1.2. $H_2C\{S(NtBu)_2(HNtBu)\}_2$ (X-ray) and $H_2C\{S(NMe)_2(HNMe)\}_2$ (Theory) (2). The geometrical arrangement of **2** (Figure 1) and its textbook Lewis structures (Scheme 1) reveal two chemically different nitrogen centers (N1 vs N2/N3). Due to the low molecular symmetry of the system, smaller differences can also occur between N2 and N3.

The S1—N1 bond in **2** shows almost the same properties as the S1—N1 bond in **1** (Table 2). Both reveal low electron density, low ellipticity, and, particularly, for the calculations, a distinct negative Laplacian at the respective BCPs as expected for single bonds. The short formal double bonds S1═N2 and S1═N3 are distinguishable from S1—N1 with respect to the absolute values of the electron density at the BCPs, but as discussed before, for the former one, the positions of the theoretical and experimental BCPs differ and as a consequence the corresponding Laplacians as well as the ellipticities cannot be compared directly (Table 2). Therefore, information about the hybridization state and the bonding of the sulfur and nitrogen atoms in **2** has to be deduced from an investigation of the spatial distribution of $\nabla^2\rho(\mathbf{r})$. As already discussed previously,[20] the experiment obviously indicates sp^3 hybridized nitrogen and sulfur atoms since, for the former well resolved lone pair related VSCCs are found (Figure 5a−g). They are notably inclined toward the sulfur atom, again testifying to lone-pair back-bonding leading to bond strengthening and shortening. Theory and experiment agree in the spatial distributions of $\nabla^2\rho(\mathbf{r})$ around N1, N2 (Figure 5e, f, h, i) and S1, but for N3 only one nonbonding VSCC could be identified by a (3, −3) cp in the theoretical $-\nabla^2\rho(\mathbf{r})$ (Figure 5g vs 5j). This can neither be assigned to a basis set deficiency (employment of the larger basis set 6-311++G** yielded the same results) nor to the slight differences in geometrical features. However, the differences are only marginal, since the theoretical spatial distribution of $-\nabla^2\rho(\mathbf{r})$ in the lone-pair region of N3 is of a distinct banana shape which also indicates at least partial sp^3 character.

The NBO/NRT analysis for $H_2C\{S(NtBu)_2(HNtBu)\}_2$ (**2**) had to be performed for $MeS(NMe)_2(HNMe)$ as a model due to convergence problems of the NRT procedure in **2**. However, the geometry of the model compound is almost identical to the main residue in **2**. Thus, both possess very similar electronic

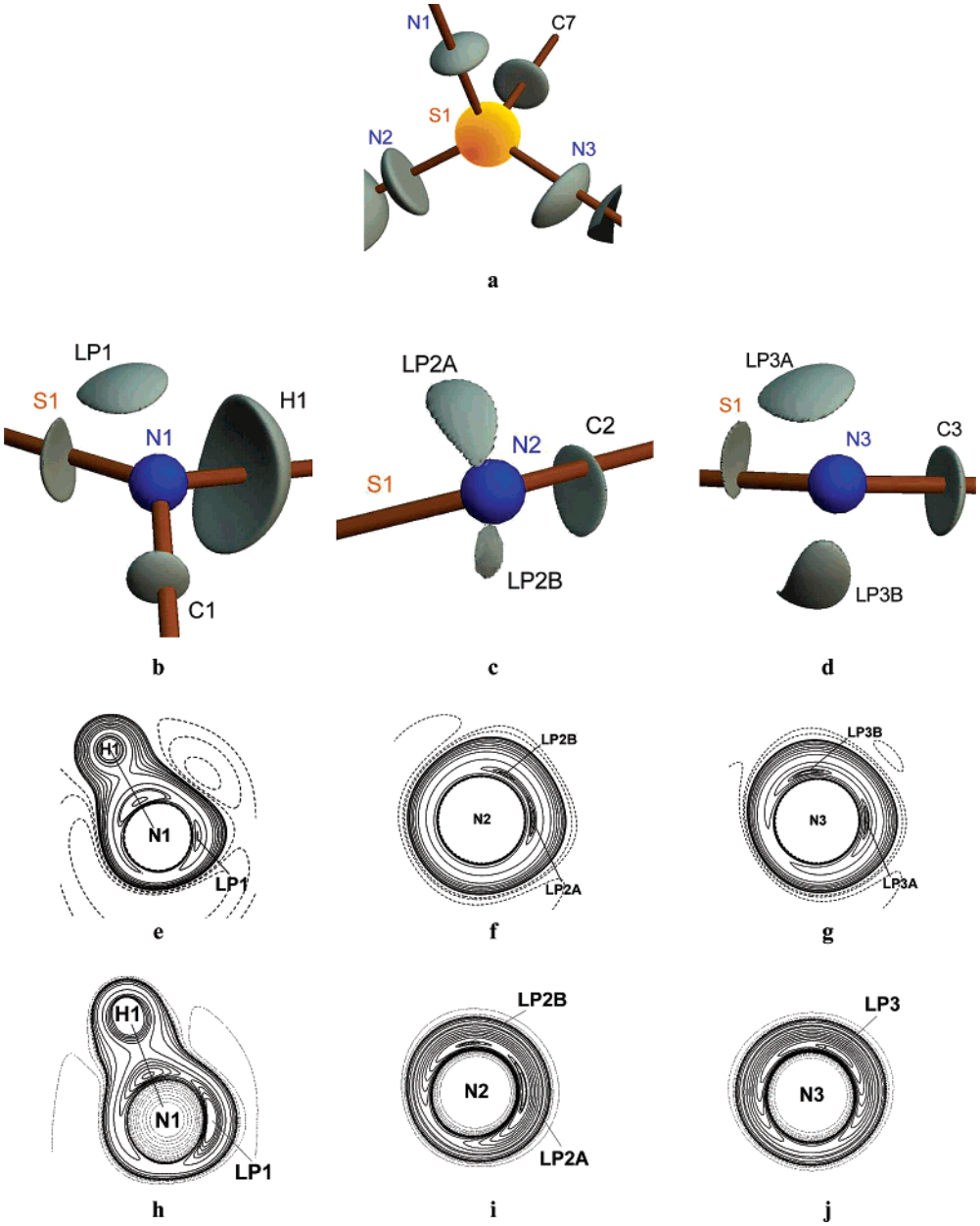

Figure 5. Isosurface ((exptl) a−d) of $-\nabla^2\rho(\mathbf{r})$ and contour plot representations ((exptl) e−g, (theo) h−j) of $\nabla^2\rho(\mathbf{r})$ (solid lines negative, dashed lines positive values) around S1 (a), N1 (b, e, h), N2 (c, f, i), and N3 (d, g, j) in **2**.

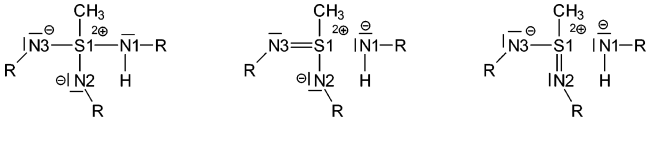

Figure 6. NBO/NRT analysis of $MeS(NMe)_2(HNMe)$ to elucidate the bonding in **2**. Formal atomic charges: (S1) +1.89 e, (N1) −1.05 e, (N2) −1.13 e, (N3) −1.12 e. Bond orders: (S1−N1) 0.67 (covalent 0.44, ionic 0.23), (S1−N2) 1.11 (covalent 0.84, ionic 0.26), (S1−N3) 1.30 (covalent 0.93, ionic 0.37), (S1−C3) 0.90 (covalent 0.89, ionic 0.01).

structures in the SN moieties. The NBO/NRT analysis gives three leading Lewis structures which cover 75% of the electron distribution not unambiguously assigned to a single canonical formula (Figure 6) and describe a situation comparable to **1**. The leading configuration supports the AIM results and experimental density distributions (Figure 5): sp^3 hybridization of S and all N atoms and consequently no S═N double bonds but ionic contributions instead. The two additional Lewis structures (Figure 6b, c) confirm that the ionic character already detected in **1** again is found in all SN bonds of **2**. For **1** and **2**, comparable formal charges and bonding characters are computed by the NBO/NRT approach. According to the formal oxidation state +VI of the sulfur atom, the formal charge of the sulfur atom changes to roughly +2 instead of +1 in the first. An inspection of the topological parameters given by the AIM procedure shows **2** to be similar to **1**. For experiment and theory the short SN bonds reveal increased density at the BCPs. Similar discrepancies as in **1** for the theoretical and experimental $\nabla^2\rho(\mathbf{r}_{BCP})$ and ϵ_{BCP} are observed in **2** resulting from differing positions of the BCPs in the SN bonds. Nevertheless, our investigations show that the SN interaction in **2** is similar to the S^+-N^- bonding in **1**.

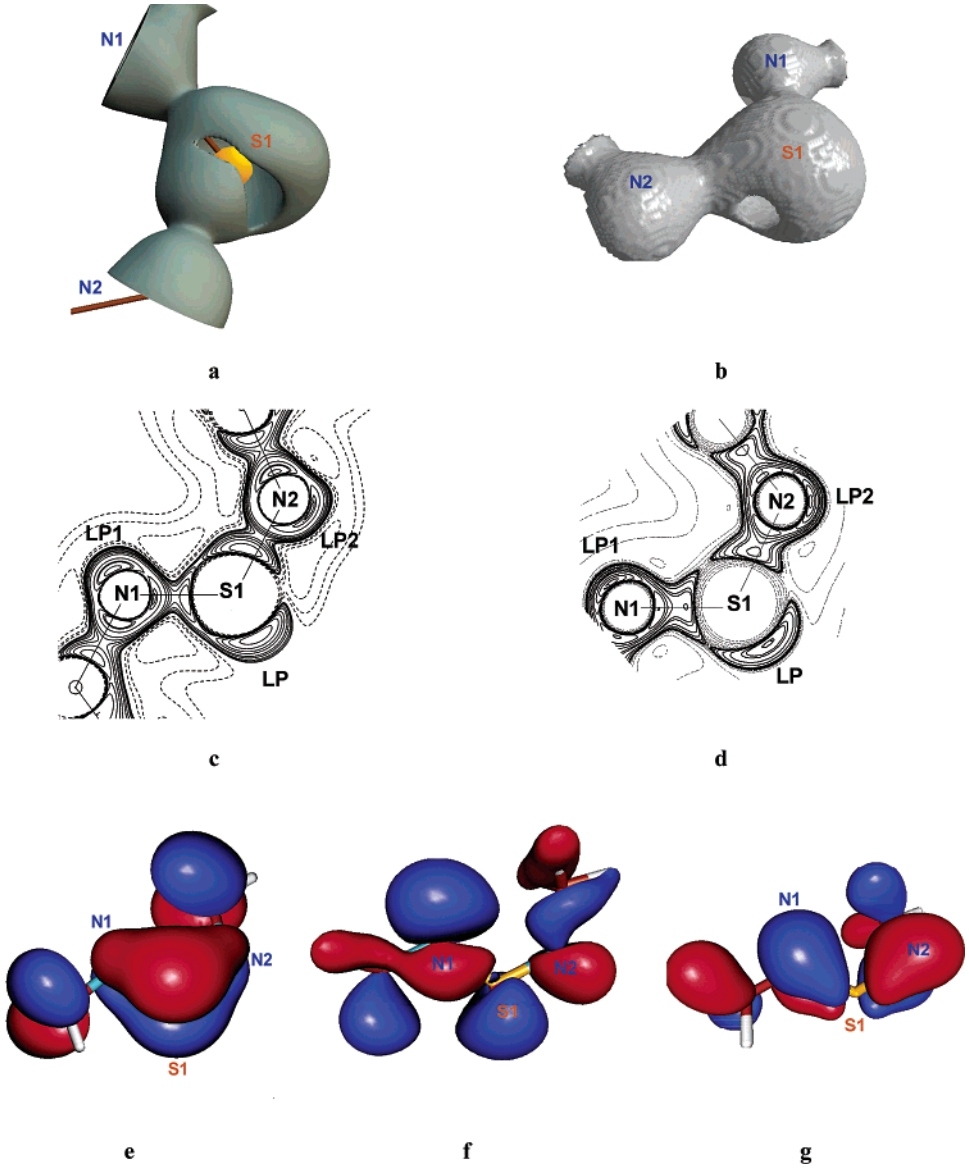

Figure 7. Reactive surfaces ($\nabla^2\rho(\mathbf{r}) = 0$; exptl, a; theo, b), experimental (c) and theoretical (d) distributions of $\nabla^2\rho(\mathbf{r})$ in the SN_2 plane, and molecular orbitals (e, HOMO-3; f, HOMO-1; and g, HOMO) of **3**.

In **1** the differing redistribution of the charge concentration at N2 in the theoretical model was attributed to the neglected solid-state environment. These effects are assumed to be small since in **1** the first coordination sphere around the negatively charged N2 was taken into account (intermolecular hydrogen bond). For a molecule of **2**, however, only the first coordination sphere of N2 is adequately described (intramolecular hydrogen bond), while, for N3, which is imbedded in a polarizing crystal field in the solid state, theory only mimics the vacuum. Computations to evaluate this effect are under way.

5.1.3. S(N*t*Bu)$_2$ (X-ray) and S(NMe)$_2$ (Theory), 3. Due to the conformation (*E*/*Z* vs *E*/*E* or *Z*/*Z*), **3** possesses two slightly different N centers (Figure 1), but in the canonical form (Scheme 1) both are doubly bonded to the sulfur atom. The calculations on S(NMe)$_2$ give two SN bonds with almost identical topological parameters. In contrast, the experimental results for the two corresponding bonds in S(N*t*Bu)$_2$ differ remarkably. However, as discussed above, the theoretical findings seem to be more reliable, since the refinement of **3** and the resulting topological values at the BCP of S1═N1 break ranks (Figure 2 and Table 2). Based on the theoretical findings, the values of $\rho(\mathbf{r}_{BCP})$ at both SN vectors are comparable to the short SN bonds of **1** and **2**. However, experimental as well as theoretical Laplacian distributions reveal only one single in-plane oriented lone-pair VSCC at both nitrogen centers and at the sulfur atom indicating primarily sp^2 hybridization (Figure 7c, d). This finding visualizes the major difference between **3** and **1** or **2** for which an sp^3 hybridization is assumed.

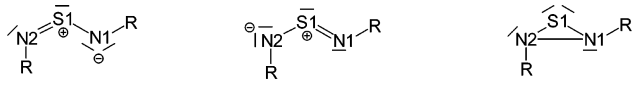

Figure 8. NBO/NRT analysis of **3**. Formal atomic charges: (S1) +1.11 e, (N1) −0.71 e, (N2) −0.77 e. Bond orders: (S1−N1) 1.49 (covalent 1.04, ionic 0.45), (S1−N2) 1.33 (covalent 0.98, ionic 0.35).

The sp^2 hybridization in the planar SN_2 core of **3** allows the formation of *m*-center-*n*-electron bonds first discussed by Rundle.[10a] Indeed, an inspection of the orbitals (Figure 7e−g)

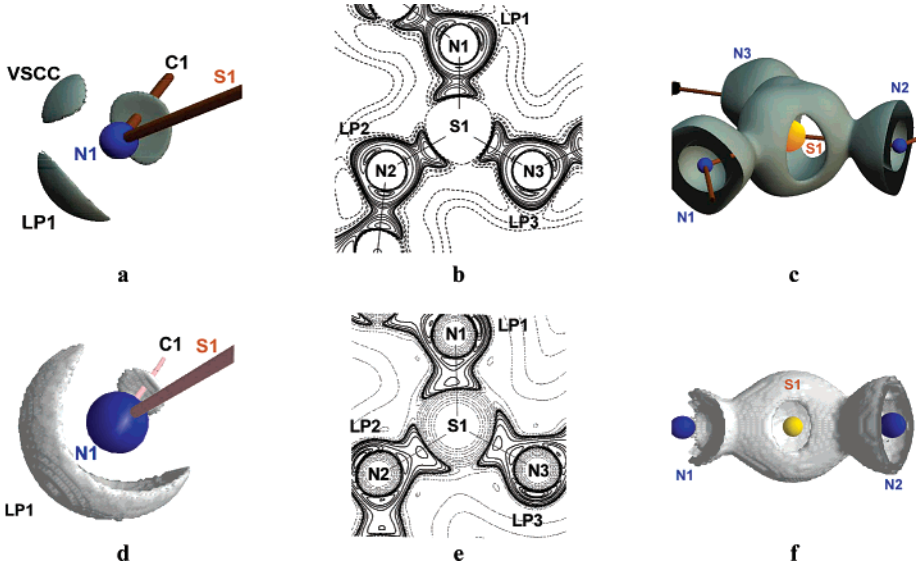

Figure 9. Isosurface (exptl, a; theo, d) and contour representation (exptl, b; theo, e) of $\nabla^2\rho(\mathbf{r})$, reactive surfaces (exptl, c; theo, f).

shows two occupied π-orbitals in **3**, which support the formulation of a 3-center-4-electron bond. However, the shape of the orbitals supports a strong polarization as it was also found for the σ-system of **1** and **2**.

The same bonding pattern results from the NBO/NRT analysis (Figure 8). The two leading resonance structures reflect the delocalization of the charge due to the 3-center-4-electron bonding in combination with a distinct polarization of the π-system. Surprisingly, the third leading Lewis structure (weight 10.5%) reveals a weak N−N bonding. This could result from the lowest π-orbital (Figure 7e), but its contribution to the bonding with respect to both N atoms is canceled by the second occupied π-orbital (Figure 7g), which is of antibonding character with respect to both nitrogen centers. The unexpected N−N bond, which was not deducible from the Bader analysis, is presumably formed by the HOMO-1 orbital (Figure 7f), which reveals a bonding in-plane π-character between the nitrogen atoms. The N−N bonding in **3** is chemically most plausible as the thiadiaziridines, containing an SN_2 heterocycle, is a well established class of compounds from the early 1970s. First established for the dioxides $O_2S(NR)_2$,[59] later the sulfur(IV) three-membered rings were synthesized.[60] However, in O_2S-$\{N(C(Me)_2CH_2tBu)\}_2$, the only structurally characterized compound,[59c] the N−N bond of 1.67 Å is considerably shorter than the N···N distance of 2.625 Å in **3**. Thus this N···N interaction is expected to be quite weak. The differences found between **1** and **2** (sp^3 hybridization of N and S, redistribution of charge through back-donation) and **3** (sp^2 hybridization, delocalization through a 3-center-4-electron bond) are reflected in the computed bond orders (Figures 4, 6, and 8, respectively). In **3** the higher bond orders (about 1.5 vs 1.1−1.2) result from an increase of the covalent (1.04 vs 0.8−0.9) as well as the ionic contributions (0.45 vs 0.2−0.3). Obviously, the redistribution of charge via a delocalized π-system is more efficient than by the back-bonding effect of both lone pairs discussed in **1** and **2**. This can also be seen from the formal charges of both nitrogen centers which are considerably smaller than in **1** and **2**.

Although differences between the theoretical and experimental topological parameters are obvious, both approaches show remarkable agreement in terms of the spatial distribution of the Laplacian. This is particularly noteworthy for the nonsymmetric distribution in the areas of positive $\nabla^2\rho(\mathbf{r})$ around the sulfur atom which reveals an open reactive surface at the *ZZ*-side of S1 (Figure 7a, b). This spatial distribution of the reactive surface ($\nabla^2\rho(\mathbf{r}) = 0$) is in ideal accordance with the observed reactivity, e.g., from the reactions of sulfurdiimides with organometallics.

5.1.4. $S(NtBu)_3$ (X-ray) and $S(NMe)_3$ (Theory), 4. Together with the S1—N3 bond of **2**, the three equivalent S—N bonds of **4** (Figure 1) are the shortest of all S—N bonds under study (Table 1). Due to its noncrystallographic C_{3h} symmetry, **4** can be formulated either as a hypovalent species (i.e., forming less bonds than expected by valence bond theory) with three S^{3+}—N^- bonds or as a hypervalent (i.e., forming more bonds than expected by valence bond theory) molecule with S═N double bonds (Scheme 1). In the theoretical density distribution of $S(NMe)_3$, all nitrogen atoms reveal one single in-plane oriented lone-pair VSCC indicating sp^2 hybridization as already observed in **3** (Figure 9d, e). In contrast, the experimental density distribution in $S(NtBu)_3$ leads to two (3,−3) cp in $-\nabla^2\rho(\mathbf{r})$. One is oriented in the SN_3 plane, while the second is positioned almost perpendicular to it (Figure 9a). To test for model dependencies, several levels of theory were employed but no qualitative changes were found. For an investigation of substituent effects, we calculated $S(NtBu)_3$, but again, just marginal changes in the density distribution around S and N were detected. The influence of the geometry was also checked. An analysis at the optimized theoretical as well as experimental geometry reveals no relevant change concerning number and position of the (3, −3) cp in $-\nabla^2\rho(\mathbf{r})$. Since the computed density is converged with respect to the approach, the differences between experiment and theory have to be assigned either to the experimental density model (disorder) or to the neglect of the crystal environment in the theoretical calculations. However,

(59) (a) Chang, H.-H.; Weinstein, B. *J. Am. Chem. Soc.* **1973**, *95*, 397. (b) Timberlake, J. W.; Hodges, M. L. *J. Am. Chem. Soc.* **1973**, *95*, 634. (c) Trefonas, L. M.; Cheung, L. D. *J. Am. Chem. Soc.* **1973**, *95*, 636. (d) Quast, H.; Kees, F. *Tetrahedron Lett.* **1973**, *19*, 1655. (e) Quast, H.; Kees, F. *Chem. Ber.* **1977**, *110*, 1780. (f) Timberlake, J. W.; Alender, J.; Garner, A. W.; Hodges, M. L.; Ozmeral, C.; Szilagyi, S.; Jacobus, J. O. *J. Org. Chem.* **1981**, *46*, 2082.

(60) (a) Kumar, R. C.; Shreeve, J. M. *J. Chem. Soc., Chem. Commun.* **1983**, 658. (b) Kumar, R. C.; Shreeve, J. M. *Inorg. Chem.* **1984**, *23*, 238.

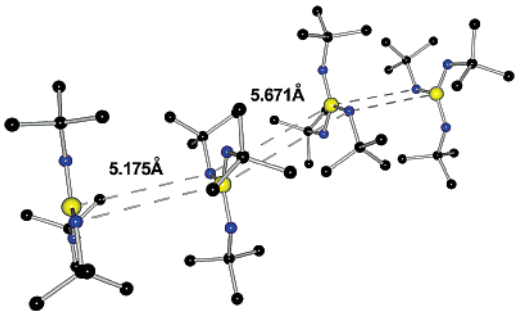

Figure 10. Packing of S(N*t*Bu)$_3$ (**4**) in the solid state; hydrogen atoms are omitted for clarity.

it is pointed out that the theoretical $\nabla^2\rho(\mathbf{r})$ distributions in the lone-pair regions of the nitrogen atoms are of a distinct banana shape (Figure 9d). Therefore, the difference between one or two separated VSCCs is regarded to be only a gradual one. Nevertheless, the theoretical distribution is symmetric relative to the SN_3 plane, while the experimental lone-pair regions show preferential orientation toward the closest neighbor in crystal packing (Figure 10).

Apart from the bare number of nonbonding VSCCs, theory and experiment are in accordance concerning the other bonding features: high densities and unprecedented distinct ellipticities of the formal S═N bonds. The spatial distributions of the Laplacian around the sulfur atom correspond also very well. This indicates that the reasons leading to the differences discussed above do not influence the electronic properties to a large extent. One example is the equal shape of experimentally and theoretically derived reactive surfaces presented in Figure 9c and f, respectively. They explain perfectly the reactivity of **4**. The reactive surface shows areas of strong charge depletion in the SN_3 plane at the bisections of the N−S−N angles at the sulfur atom. Interestingly, differing from the distribution in **3** (Figure 7a), there is no hole in the reactive surface on top or underneath the sulfur atom. This, in fact, explains the reactivity of the sulfurtriimide: S(N*t*Bu)$_3$ reacts smoothly with MeLi,[12a] PhCCLi,[14] SC_4H_3Li,[61] or $SC_4H_2Li_2$[62] but not with *n*BuLi or *t*BuLi. The carbanionic nucleophile has to approach the sulfur atom along the NSN bisection in the SN_3 plane or in an angle of less than about 45° which is only feasible for small or planar carbanions. Bulky anions cannot reach the holes, due to the steric hindrance of the N*t*Bu groups. The steric argument would not be valid if a direct orthogonal attack above or underneath the SN_3 plane was favored, as there is sufficient space in the planar molecule to reach the sulfur atom directly.

As for **3**, the symmetry of **4** allows the formation of a π-system perpendicular to the SN_3 plane. This is indeed found. The occupation pattern of the orbitals indicates a 4-center-6-electron bonding (Figure 11).

The NBO/NRT analysis supports the same interpretation. It gives one leading, triply degenerated resonance structure (Figure 12), which covers 75% of the distributed electronic structure. These Lewis structures reflect the delocalization effects due to the 4-center-6-electron bonding in combination with a distinct polarization of the π-system. The computed bond orders are slightly smaller than in **3**. Contrary to **3**, no bonding between the nitrogen atoms is found. The reason may be the lack of the

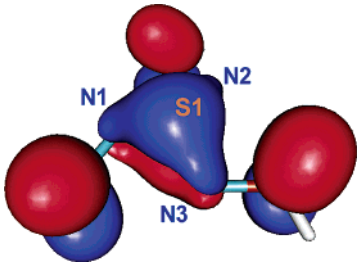

Figure 11. HOMO-5 in **4**.

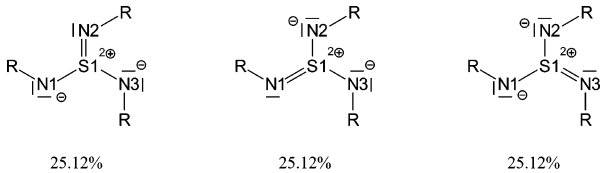

Figure 12. NBO/NRT analysis of **4**. Formal atomic charges: (S1) +1.90 e, (N) −0.63 e. Bond orders: (S−N) 1.33 (covalent 0.97, ionic 0.35).

in-plane π-orbital, which is responsible for the bonding in **3**. The interpretation given by the NBO/NRT analysis (polarized SN bonds accompanied by delocalization effects via a 4-center-6-electron bonding) is in accordance with the findings of the AIM approach which gave sp^2 hybridized centers, high densities, and unprecedented distinct ellipticities at the BCPs for both theory and experiment.

The disagreement between experiment and theory about the number of VSCCs around the nitrogen centers could result from the possible disorder in the solid state discussed above or from crystal field effects, which are not taken into account in the theoretical model. In the solid state, the S(NtBu)$_3$ molecules are oriented in a staggered ladder structure (Figure 10). Each sulfurtriimide molecule is surrounded by two coplanar neighboring units. One is in relative close proximity (5.175 Å) connected via a center of inversion. The other neighbor is located in a distance of 5.671 Å. The out-of-plane VSCC at the nitrogen atoms point toward the closest neighboring electrophilic sulfur atom in the S−N···S−N stack. Therefore, this charge concentration might not indicate a lone pair but a perturbation in the delocalized π-system. Computations which mimic such effects to study their influence at the density distribution around the nitrogen centers are under way.

6. Conclusions

In the present paper, the charge density distribution in the four sulfur−nitrogen compounds methyl(diimido)sulfinic acid H(N*t*Bu)$_2$SMe (**1**), methylene-bis(triimido)sulfonic acid H_2C-{S(N*t*Bu)$_2$(HN*t*Bu)}$_2$ (**2**), sulfurdiimide S(N*t*Bu)$_2$ (**3**), and sulfurtriimide S(N*t*Bu)$_3$ (**4**) was determined by high-resolution X-ray diffraction experiments and theoretical approaches. Good agreement between experimental and theoretical results was obtained for the geometrical properties and for the qualitative features of the spatial distribution of the Laplacian (shape of $\nabla^2\rho(\mathbf{r})$, number and positions of nonbonding VSCCs). One exception (the S1−N1 bond in S(N*t*Bu)$_2$) was related to shortcomings in the experimental model. The reason for the other discrepancy between theory and experiment (number of VSCCs at the nitrogen centers of S(NR)$_3$) remains unclear since it could be induced by the crystal field. However, the deviations are just marginal. Calculations to study this effect are under

(61) Selinka, C.; Stalke, D. *Z. Naturforsch.* **2003**, *58b*, 291.
(62) Selinka, C.; Stalke, D. *Eur. J. Inorg. Chem.* **2003**, 3376.

way. Large differences between theory and experiment are found if the comparison was restricted to the eigenvalues of the Hessian matrix at the BCPs. Particularly λ_3 deviates strongly. This well-known mismatch between theory and experiment arises mainly from the different positions of the theoretical and experimental BCPs in the short SN bonds. Nevertheless, the charge densities at the BCPs were found to be well correlated. Due to the deficiencies mentioned above, the bonding analyses were performed by investigating the spatial distribution of $\nabla^2\rho(\mathbf{r})$ which allowed a profound characterization of the various bond types.

As expected, all SN bonds are found to be quite polar. The bond mode of the short SN bonds is of particular interest, while the long SN bonds between sulfur and the trisubstituted nitrogen atoms doubtless represent polar single bonds. The bonding type of the short SN bonds between sulfur and the disubstituted nitrogen atoms depends on the geometrical arrangement of the SN moiety. In the classical interpretation, they are formulated as S═N double bonds but, for the species $H(NR)_2SMe$ and $H_2C\{S(NR)_2(HNR)\}_2$, respectively, in which the sulfur atoms are obviously sp^3 hybridized, AIM indicates negatively charged sp^3 nitrogen atoms with two lone pairs at each disubstituted nitrogen atom. The NBO/NRT analyses support this finding and draw a more subtle picture. A redistribution of the density from the negatively charged nitrogen centers into the SN bonds is indicated. Thus, the short SN bonds exhibit increased covalent as well as ionic contributions to the total bond order compared to the long SN bonds, which is indeed reflected by the NBO/NRT bond orders. In the AIM interpretation, the redistribution can also be deduced from the topological parameters. Furthermore, the VSCCs are found to be oriented toward the sulfur centers leading to lone-pair back-bonding. In summary, the investigations show that the short bonds of **1** and **2** should be formulated as $S^+—N^-$ rather than as an S═N double bond. Valence expansion to more than eight electrons at the sulfur atom, however, can definitely be excluded to explain the bonding.

In the planar species $S(NR)_2$ (**3**), and $S(NR)_3$ (**4**), the analyses of the spatial distributions of $\nabla^2\rho(\mathbf{r})$ reveal sp^2 hybridization for all S and N atoms. This indicates a π-system above and below the SN_x plane. Such a π-system is indeed reflected by the corresponding π-orbitals and the leading resonance structures given by the NBO/NRT approach. This bonding type corresponds to the 4-center-6-electron bonding. As a consequence of the π-system, the redistribution of charge should be more efficient. Indeed, the NBO/NRT analyses reveal increased covalent contributions to the SN bond orders accompanied by decreased charges at the nitrogen atoms in **3** and **4** compared to **1** and **2**. However, from the shape of the orbitals and from the NBO/NRT resonance structures it is obvious that the π-orbitals are polarized. Thus, also the ionic contributions to the total bond orders are slightly raised in the short SN bonds of **3** and **4**. Again, valence expansion at the sulfur atom can be excluded.

In addition to the bonding type, our investigations also elucidate the experimentally observed reactivity by inspection of the reactive surfaces. For example, $S(NtBu)_3$ reacts smoothly with MeLi and PhCCLi but not with *n*BuLi or *t*BuLi. Our analysis shows that this discrimination of large reactants can be related to small areas of strong charge depletion in the SN_3 plane at the bisections of the N−S−N angles.

Acknowledgment. This work was supported by the Deutsche Forschungsgemeinschaft (Graduiertenkolleg 690: Elektronendichte, Theorie und Experiment) and the Fonds der Chemischen Industrie. Support of BRUKER Nonius, Karlsruhe, and CHEMETALL, Frankfurt/Main, is kindly acknowledged. The authors thank Dagmar Ilge for fruitful discussions.

Supporting Information Available: Experimental Section: data collection and processing, crystal data tables for **1**−**4**, details of mulipole refinements including atomic coordinates after multipole refinement, local coordinate systems, multipole populations, residual density bond lengths and angles, anisotropic displacement parameters, bond critical points, critical points in the Laplacian distribution around the nitrogen atoms. Theoretical Section: atomic coordinates of optimized geometry, critical points, eigenvalues. X-ray crystallographic data for **1**−**4** in cif file format are available. This material is available free of charge via the Internet at http://pubs.acs.org.

JA038941+